William & Mary

Investigating Side Chain Dynamics of Host Defense Peptide Piscidin 1 Using ^{2}H Solid-State NMR

Ryan Sell

Advisor: Professor Myriam L. Cotten

Abstract

Host Defense Peptides (HDPs) are present in immunological systems and possess a wide variety of antimicrobial properties. In researching the ways in which HDPs interact with their environment and the cells that they target, we have the potential to inform on key characteristics that could be instrumental in the development of new sources of immunologically defensive agents. The Piscidin family of HDPs has shown remarkable potential in effecting drug-resistant bacteria [1, 2]. The isoforms of Piscidin, namely Piscidin 1 and Piscidin 3 (p1 and p3) are homologous and both bind to copper ions [1]. Their general mechanism is concentration-dependent and involves orientation parallel to the membrane surface at low concentrations (e.g. a bacterial cell membrane), followed by membrane destabilization, and lysis or degradation of the target cell at high concentrations [3]. The form p1, but not p3, has a phenylalanine amino acid residue at position 2 (F2). F2's position as an aromatic side chain could stabilize the metal when the peptide inserts into the hydrophobic lipid membrane. Solid-state nuclear magnetic resonance (ssNMR) analysis of F2(d5)-p1, p1 with a deuterated F2 side chain, has the capacity to reveal rotational behavior due to the sensitivity of deuterium NMR to the time scale and symmetry of molecular motion. By iterating the main deuterium signal NMR components through parameters in molecular dynamics simulations and comparing the resulting NMR spectra with experimental NMR spectra from the F2(d5)-p1 runs, we can explore the rotational behavior and conformational changes of the phenylalanine at this position to investigate how metal coordination is influenced by neighboring side chains and the lipid environment.

Acknowledgements

I would like to express thanks to Dr. Myriam Cotten for instructing and informing me throughout my learning of physical studies of biochemical samples, as well as for the steady advice and hard work put into helping me deliver this thesis. I would like to thank Dr. Alex Greenwood for teaching me how comprehensive the structural studies of NMR are, how to qualitatively interpret and assess data, and for running all of the NMR experiments involved in this project. I would like to thank Dr. Yimin Miao for supervising me, preparing samples involved, and answering my many questions. I would also like to thank the entirety of the Cotten group for their support, advice, and teaching this year.

Contents

Abstract **i**

Acknowledgements **iii**

1 Introduction **1**

1.1 Host Defense Peptides 1

1.2 Piscidin 2

1.3 Piscidin Structure 3

1.4 Model Membranes 4

1.5 Amino Terminal Cu(II)- and Ni(II)-Binding Motif 5

1.6 Reactive Oxygen Species 6

1.7 Nuclear Magnetic Resonance 7

1.8 Deuterium NMR 13

1.9 Features of Deuterium NMR 15

1.10 Magic Angle Spinning (MAS) 16

1.11 Structural Analysis of P1 17

2 Experimental Approach **19**

2.1 Peptide Synthesis & Purification 19

2.2 Data 20

2.3 ^{2}H NMR Data Analysis 24

2.4 Results 26

3 Conclusion **29**

3.1 Summary 29

3.2 Applications 29

3.3 Future Work 30

Bibliography **31**

Chapter 1

Introduction

1.1 Host Defense Peptides

The human immune system can be broken down into two components, the innate and the adaptive. The innate immune system responds immediately to possible infection with non-specific responses, while the adaptive immune system registers an immunological memory to each pathogenic event and modulates specific responses to pathogens it can recognize. Innate immunological responses are non-specific in that they attack (or prevent the permeation of) foreign cells indiscriminately. Commonly recognized constituents of the innate immune system include the skin, saliva or mucus, and inflammation, as they deter or lead to the death of pathogens that would otherwise integrate into the body.

Host Defense Peptides (HDPs, also known as antimicrobial peptides) are molecular components of this innate system. HDPs have antimicrobial properties, a wide range of efficacy, and utilize mechanisms that do not incur high rates of bacterial resistance [1]. The majority are broadly antimicrobial and cationic at physiological pH [4]. Their cationic nature is significant in that they target anionic bacterial membranes. The general mechanism of p1 involves binding of the HDP more or less parallel (at a particular orientation that varies depending on the peptide in question) to the bacterial membrane surface at low concentrations, and membrane destabilization induced lysis at high concentrations. Further analysis is required to build a

complete understanding of HDPs' mechanisms of action. International interest has turned to exploring new methods of treating harmful microbes due to the rise of drug-resistant bacteria, especially "super-bugs" like Methicillin-resistant *Staphylococcus aureus* (MRSA). Methicillin is one of many antibiotics whose extensive use in the past 70 years has led to the untreatable bacterial infections plaguing the modern medicinal landscape [5]. Thus, it is promising that Piscidin, the family of HDPs studied in the Cotten lab, clearly exhibits anti-bacterial activity in a wide range of "Gram-positive" and "Gram-negative" bacteria, which includes MRSA. These peptides additionally act against viruses such as the Human Immunodeficiency Virus (HIV), cancer, and fungal infections [1, 6, 7]. Research into the naturally occurring homologues of Piscidin, as found in teleost fish [8], could help the scientific community understand characteristics that could be key in developing novel agents necessary to counter threats such as drug resistance to viral, bacterial, and fungal infections, as well as tumors.

1.2 Piscidin

The focus of work in Dr. Cotten's lab has been on two conformations of the Host Defense Peptide Piscidin. Each homologue, Piscidin 1 and Piscidin 3 (p1 and p3) is 22 residues in length [1]. The amino acid sequences of p1 and p3 are conserved: that is, 13 (out of 22) residues share the same position between the two peptides (see figure 1.1). The minimum inhibitory concentration (MIC) of a peptide is defined as the lowest concentration of an antimicrobial (p1 or p3) that will inhibit the visible growth of a microorganism overnight incubation [9]. The MICs for the peptides exhibit p1 having stronger antimicrobial effects than p3 (see table 1.1) [1].

	p1 concentration (μM)	p3 concentration (μM)
Escherichia coli (E. coli)	2-10	10-20
Bacillus cereus	$\leq$2	2-10

Table 1.1: Minimum inhibitory concentrations of p1 & p3 [1].

A distinguishing feature of Piscidins compared to other HDPs is that they contain tenfold the average % of histidine residues reported within the Antimicrobial Peptide Database (the

P1	**FFHHIFRGIVHVGKTIHRLVTG**
P3	**FIHHIFRGIVHAGRSIGRFLTG**

Figure 1.1: Bold amino acid residues between p1 and p3 indicate conservation (the presence of residues that are found at identical sites in each peptide chain) [1, 10].

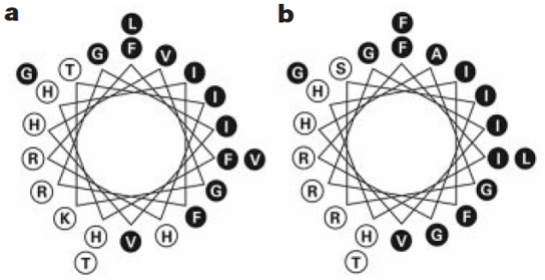

Figure 1.2: Wheel structure depicting the α-helical structures of (a) p1 and (b) p3. The filled-in amino acids are hydrophobic and the empty amino acids are hydrophilic. Figure from [8].

APD) [10]. Histidine has a characteristic pH of 6.0, close to physiologically relevant pH values (e.g. pH of human blood ≈ 7.4). Consequently, due to its mostly positive charge at a pH < 6.0 and mostly neutral charge at a pH > 6.0, the presence of multiple histidines can modulate the overall shape of the peptide. For example, the peptide LAH_4 exhibited oriental changes from being transmembrane at an neutral pH to parallel the lipid bilayer at an acidic pH [11]. In this sense, the peptide charge is pH-regulated. This is significant in consideration of the peptide's intracellular (in the phagosome) and extracellular activity [12].

1.3 Piscidin Structure

The APD reports that 41% of all HDPs with recorded secondary (2°) structures have α-helical content [1, 10]. The structure of p1 and p3 is added to this list as well. Generally, the proposed reason for such a commonplace occurrence of α-helices in HDPs is the characteristic amphipathicity that can be generated by such a structure. When a structure (typically a protein, but in this case a peptide chain) is described as amphipathic, it consists of both hydrophobic and hydrophilic regions. For an α helix there are two regions (two sides), one polar and the other neutral. In a physiological environment, this sort of conformation is highly

conducive to membrane binding. The hydrophobic side of the α-helical peptide can match the membrane's hydrophobic phospholipid heads while the peptide's hydrophilic side remains facing the outside environment (see figure 1.2). The combination of oriented sample solid-state nuclear magnetic resonance (OS ssNMR), molecular dynamics (MD) simulations, and circular dichromism (CD) has achieved for p1 and p3 a high resolution three dimensional (3D) structure and orientation in addition to the α-helical motif [1, 13]. Detailed structural and orientational (with respect to the target membrane) information of the Piscidin family has the potential to illuminate the most significant components of p1 and p3's mechanisms of action, especially since only 14% of recorded HDPs by the APD have recorded 3D structures [1, 10].

1.4 Model Membranes

It is unpractical, due to the sheer amount of factors involved in a true physiological environment and organism, to determine the structure of HDPs or other such membrane-interacting peptides and proteins *in vivo*. Instead, model membranes are made from synthetic lipids to mimic biological membranes and provide a means of controlling the protein/lipid ratio, pH, ionic strength, and many other chemical factors. They closely mimic bacterial membranes, but because bacterial species vary immensely, model membranes need to be reconstituted in various compositions as well. Bacterial bilayers differ in the classes of lipids they are comprised of, thus these classes of lipids are mixed and interchanged in the construction of model membranes. It is important to take care in choosing a model membrane; a particular peptide or protein might possibly only have high affinity for one specific lipid species [14]. Among the most common lipid components of bacteria are, for example, phosphatidylethanolamine (PE) and phosphatidylglycerol (PG) [15, 16, 17]. Synthesis in a lab environment creates membranes with lipid class characteristics, for instance via the creation of 1:1 1-palmitoyl-2-oleoylsn-glycero-phosphatidylethanolamine (POPE) / 1-palmitoyl-2-oleoyl-sn-glycero-phosphoglycerol (POPG) and 3:1 1,2-dimyristoyl-sn-glycero-3-phosphatidylcholine (DMPC) / 1,2-dimyristoyl-sn-glycero-3-phosphatidylglycerol (DMPG) [1]. A 1:1 ratio of POPE:POPG and a 3:1 ratio of DMPC/DMPG were used as model membranes in the determination of the structure and

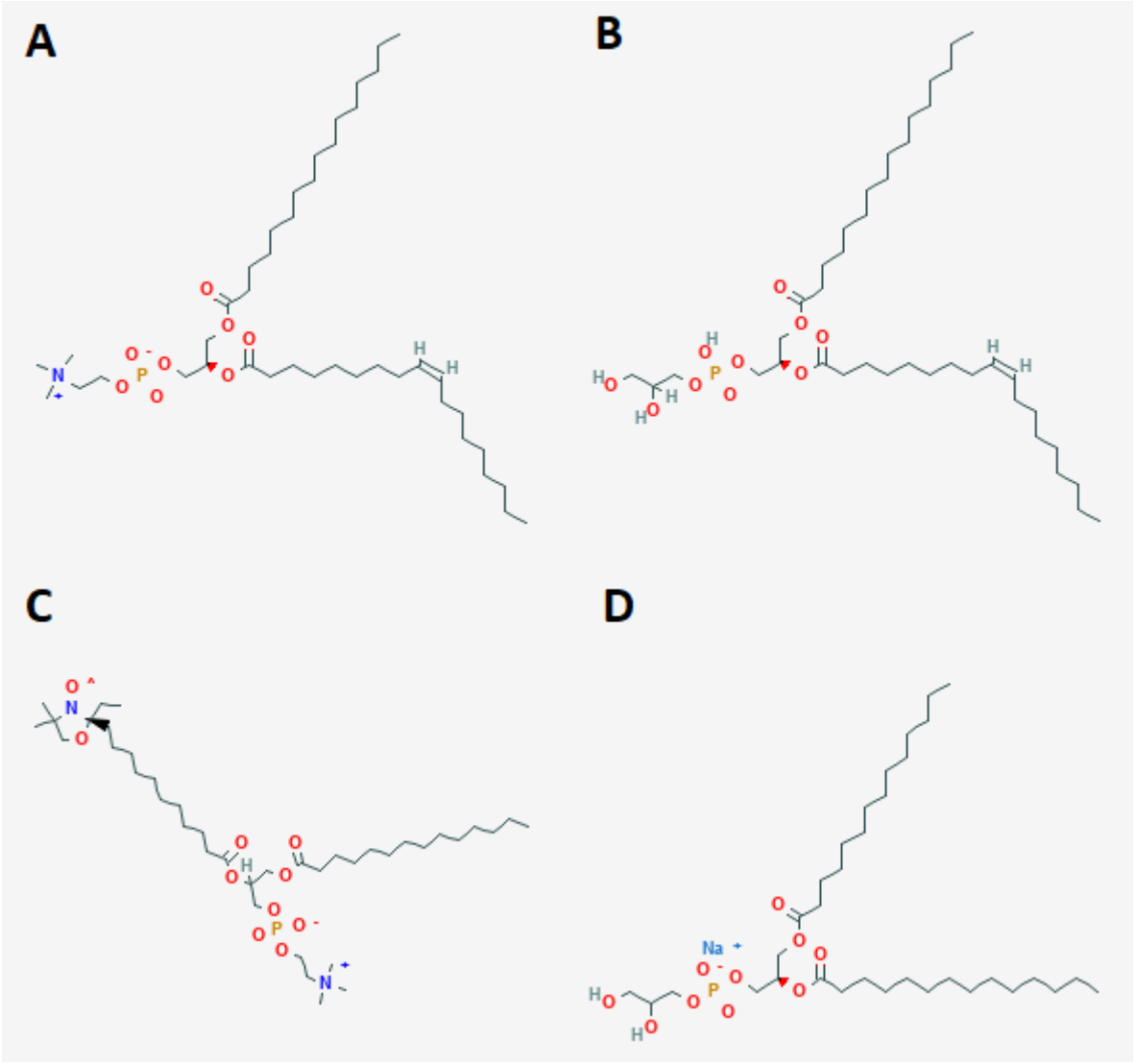

Figure 1.3: Molecular Structures of A) POPC, B) POPG, C)DMPC, and D) DMPG [18, 19, 20, 21].

orientation of p1 and p3 [1]. The molecular structures of these lipids can be seen in figure 1.3.

1.5 Amino Terminal Cu(II)- and Ni(II)-Binding Motif

The Amino Terminal Cu(II)- and Ni(II)-Binding (ATCUN) motif is a structural feature found in many HDPs and in both Piscidins; this motif is conducive to metal (copper or nickel) coordination [22, 23]. The metal is coordinated by an amino terminal nitrogen, two backbone nitrogens, and a histidine in the third position (see figure 1.4). In p1 and p3, we can see the indicator of this motif through their first three residues: FFH and FIH. Metallated HDPs

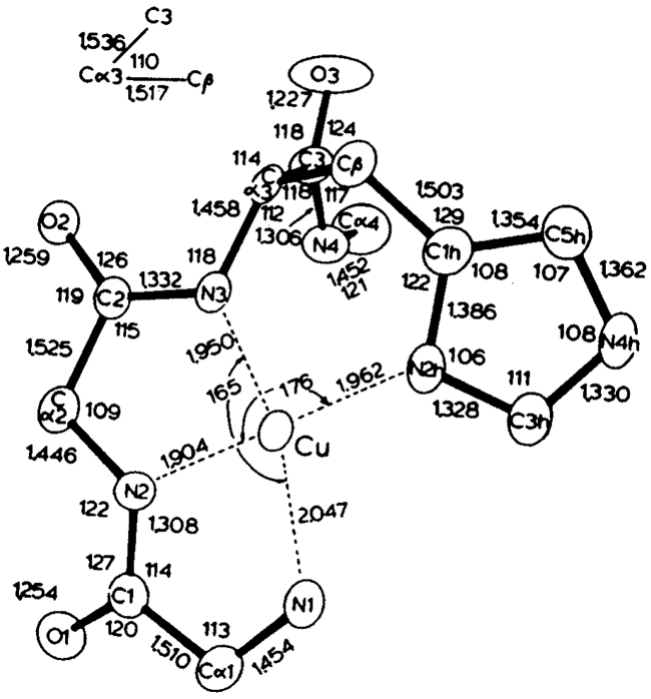

Figure 1.4: The N-terminal nitrogen is represented by N1. N2 and N3 are the following nitrogens along the peptide background. N2h is the final coordinating nitrogen by the histidine at position 3. Figure from [23].

including p1 and p3 have been shown to inflict damage on membranes and even on bacterial DNA [22, 3, 24, 25].

1.6 Reactive Oxygen Species

When HDPs coordinate copper via the ATCUN motif, Cu^{2+} can generate reactive oxygen species (ROS) as it alternates between oxidation states Cu(II) and Cu(III). Reactive oxygen species can propagate radicals through physiological environments [26]. Generally speaking, the oxidation and reduction of copper rips single electrons from involved chemical reactants. Such radicals (atoms with unpaired valence electrons) are unstable chemical forms and will therefore propagate into a reaction cascade (damaging existing cellular structures) until a stable molecule is produced with paired electrons (see figure 1.5). In the specific reactions of HDPs and their membrane targets, there is a general interpretation of the ROS mechanism. The HDPs bound to Cu^{2+} may bind to the membrane, then initiate interactions of ROS in the unsaturated fatty

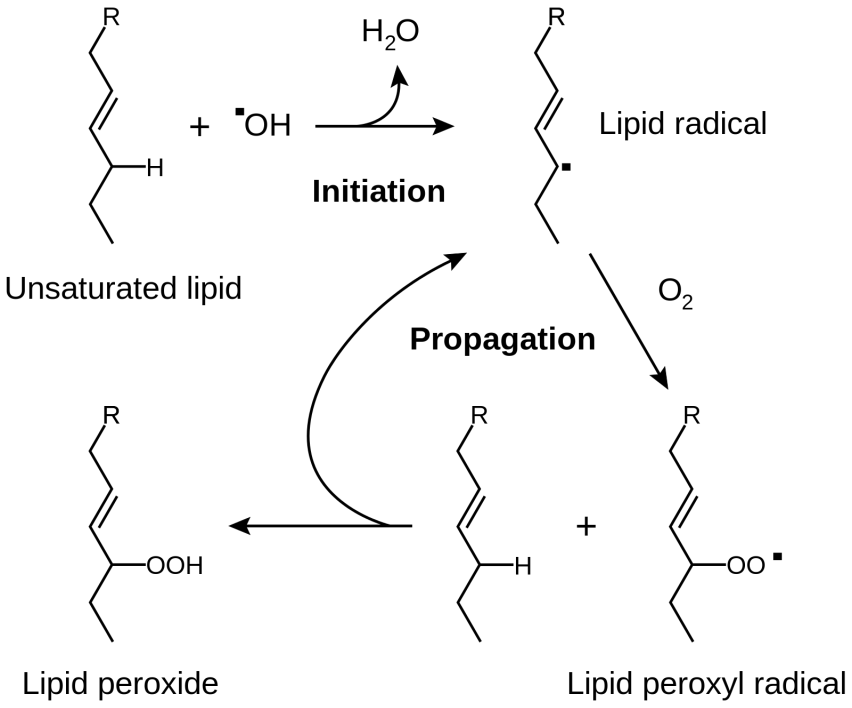

Figure 1.5: Radical initiation, propagation, and termination beginning with an unsaturated fatty acid and a hydroxyl radical. The hydroxyl radical is unstable and seeks its lost electron in the hydrogen of the unsaturated fatty acid tail. The water molecule resolves itself at the cost of generating a lipid radical. The lipid radical propagates a lipid peroxyl radical which in turn reacts with the original unsaturated fatty acid to form a lipid peroxide and propagates another lipid radical. The process continues in destabilization until reactants are consumed. Figure from [28].

acid tails (ROS oxidizes the unsaturated fatty acid's double bonds). The hydrophobic tails when oxidized become more polar and consequently perturb the membrane and make it easier to lyse. These conjoint steps ultimately destabilize the membrane via lysis [26, 27] (see figure 1.6).

1.7 Nuclear Magnetic Resonance

Nuclear Magnetic Resonance (NMR) experiments offer high resolution structural and orientational analysis of samples. NMR operates via detection of nuclei, specifically nuclear spin. Spinning nuclei have angular momentum (P), and the motion of their charge generates a

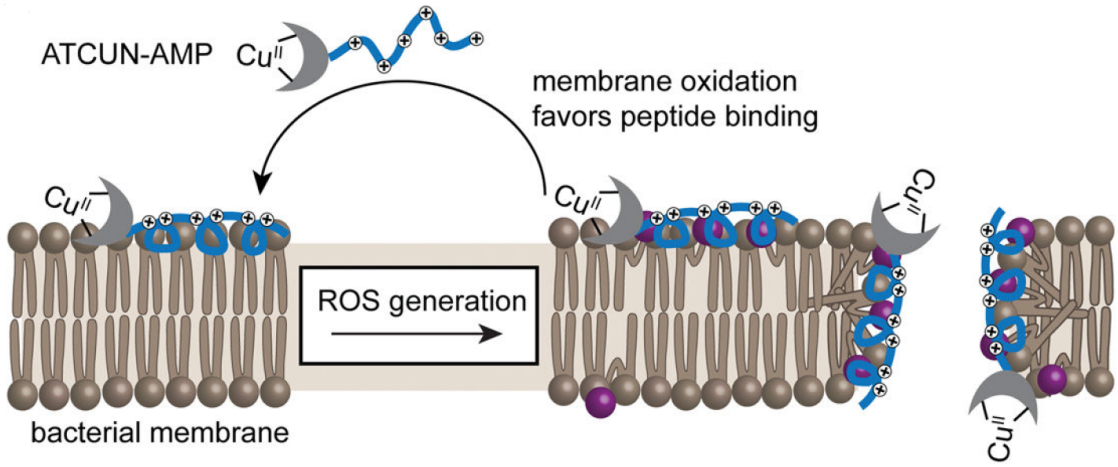

Figure 1.6: A general HDP in complex with copper via the ATCUN motif is referenced as the ATCUN-AMP (ATCUN antimicrobial peptide). The coordinated copper contributes to ROS generation and membrane disruption. Figure from [26].

magnetic moment μ which can be described by the following equation:

$$\mu = \gamma P \tag{1.1}$$

where γ is the gyromagnetic ratio [29]. When placed inside of a strong external static magnetic field B_0, there is a limited number of possible orientations due to quantised energy states. A nucleus with spin I will have $2I + 1$ spin states. Since the nuclear spin of ^{1}H is $1/2$, its states are $\pm 1/2$ (see figure 1.7). Considering figure 1.7, the β indicates the state of higher energy due to anti-parallel spin while the α indicates the state of lower energy due to parallel spin in relation to B_0. There are slightly more α state nuclei than β state nuclei (the α state is of lower energy and thus is more stable). Because there are more α nuclei, their compound magnetic moments (μs) result in a "bulk magnetization" along the $+z$ axis (see figure 1.8).

A nucleus with a nuclear spin and magnetic moment will precess inside of a strong external static magnetic field B_0. Precession is the change in the orientation of the rotational axis of a rotating body, like how the Earth is on a tilt while rotating (although its precession has a cycle of 26,000 years). Precession here in the nucleus is caused by the axis of the nucleus' magnetic moment being tilted by B_0 (see figure 1.9). The application of B_0 creates a torque in the nuclei that causes the nuclei to precess at a frequency known as the Larmor precession

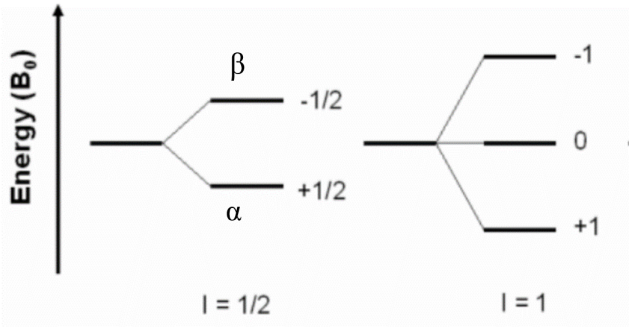

Figure 1.7: The diagram depicts the nuclear degeneracy (the available energy states) for nuclear spin ½ and 1 nuclei when placed in a static external magnetic field. Figure from [30].

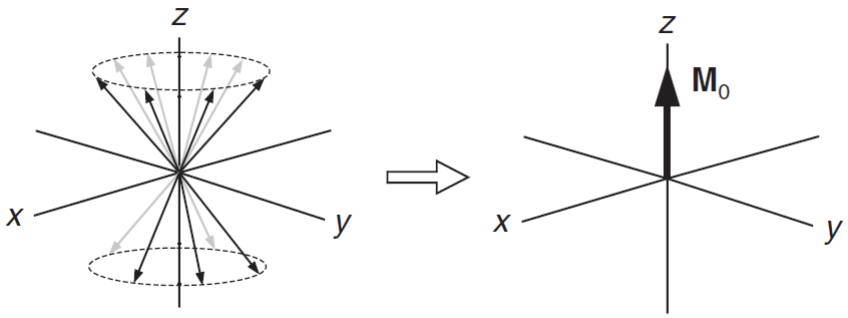

Figure 1.8: Slightly more α state nuclei than β state nuclei result in magnetic moments that sum toward the $+z$ axis (as a bulk magnetization). Figure from [29].

frequency v,

$$v = \frac{-\gamma B_0}{2\pi} \tag{1.2}$$

The nuclei still exist in both states, α and β, and with a bulk magnetization on the $+z$ axis [29]. More nuclei are in the lower energy α state. The energy gap between the states can be described by,

$$\Delta E = hv = \frac{\gamma B_0 h}{2\pi} \tag{1.3}$$

where h is Planck's constant. A radiofrequency (rf) pulse, i.e. a time-dependent oscillating field B_1, is applied perpendicular to the static magnetic B_0 in order to force the bulk magnetization from the $+z$ axis to the (x, y) plane. Physically, this is achieved by propagating the rf pulse through a coil surrounding the sample. The frequency of this pulse should match the Larmor precession to provide the appropriate energy for the bulk magnetization change (energy to shift excess α state nuclei to the β state), corresponding to equation 1.3 [29]. Only a bulk magnetization vector in the (x, y) plane induces a signal in the detection coil, which lies on the (x, y) plane as well [29]. For example, the rf pulses are applied typically with a 90° (90_x) pulse along the x-axis which aligns the bulk magnetization vector along the y-axis (see figure 1.10) [29]. The nuclei still exhibit Larmor precession (since the sample is still spinning outside of our magnetization's frame of reference), so this $+y$ axis' rotating magnetization vector produces a weak oscillating voltage in the detection coil previously mentioned surrounding the sample along the (x, y) axis. RF pulses could also be applied at 180°, though this simply inverts the nuclei populations and yields no signal. The usefulness of such a pulse would be in the realm of calibration during multiple pulse experiments. Small discrepancies exist in the frequency of the nuclei examined along the (x, y) axis due to their respective slight chemical differences (their chemical shifts). A chemical shift is the resonant frequency of a nucleus relative to the standard in a magnetic field and is described by δ in the following equation:

$$\delta = \frac{v_{detected} - v_{reference}}{v_{reference}} * 10^6 ppm \tag{1.4}$$

ppm denotes parts per million, since these discrepancies between nuclei are on the order of a thousand Hz instead of MHz it is simply a cleaner unit to work with. The frequency data from

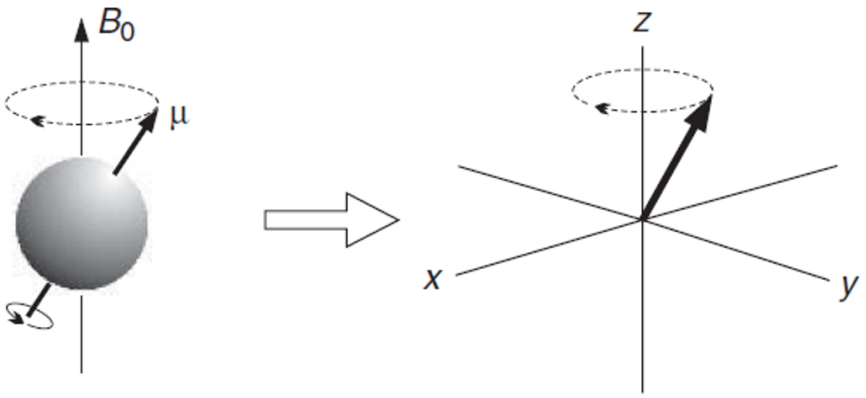

Figure 1.9: External static magnetic field B_0 with the nucleus' magnetic moment μ. The cartesian coordinate plane displays precession about the z axis. Figure from [29].

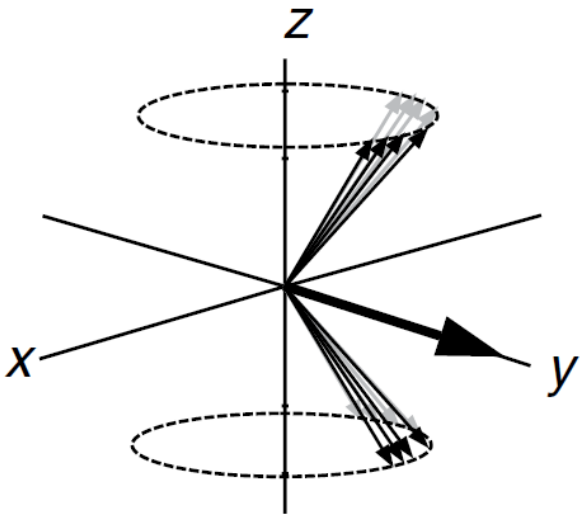

Figure 1.10: Spin vectors group along the y-axis after a 90° pulse. Figure from [29].

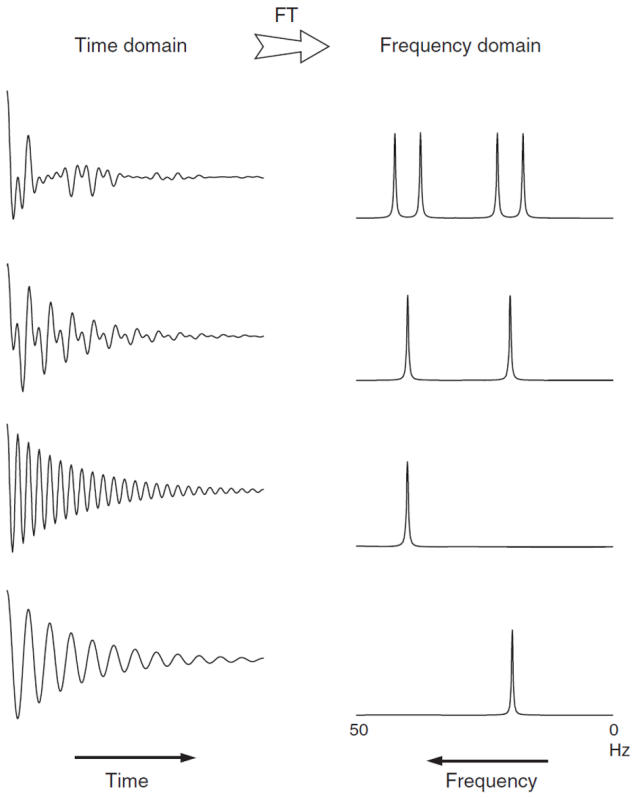

Figure 1.11: Signal data is detected in a time-dependent manner and digitized. Performing a Fourier Transform on the digitized data's FID can extract the individual frequency components contained. FT figure from [29].

the detection coil is able to detect data on this order of magnitude. Slight chemical differences arise because electrons surrounding nuclei respond to the magnetic field B_0. The precession of the nuclei (caused by B_0) induces motion of their electrons, which in turn generates a small magnetic field opposed to B_0. These small magnetic fields contribute to a diminished effective B_0 with a magnitude dependent upon the surrounding environment of particular nuclei, and thus disparate chemical shifts of nuclei. It is with this knowledge of chemical shift that we can approach a free induction decay (FID) and its associated frequency NMR spectrum. A free induction decay is the observable NMR signal generated by the data from the detection coil previously described.

A Fourier Transform (FT) is a mathematical means to extract the multiple frequency components that together form a time-domain signal. Figure 1.11 reveals a few examples.

In solution (liquid) NMR, spin dipoles are statistically distributed randomly, in contrast to oriented sample NMR. The NMR spectra of solid-state NMR can reveal a distribution of

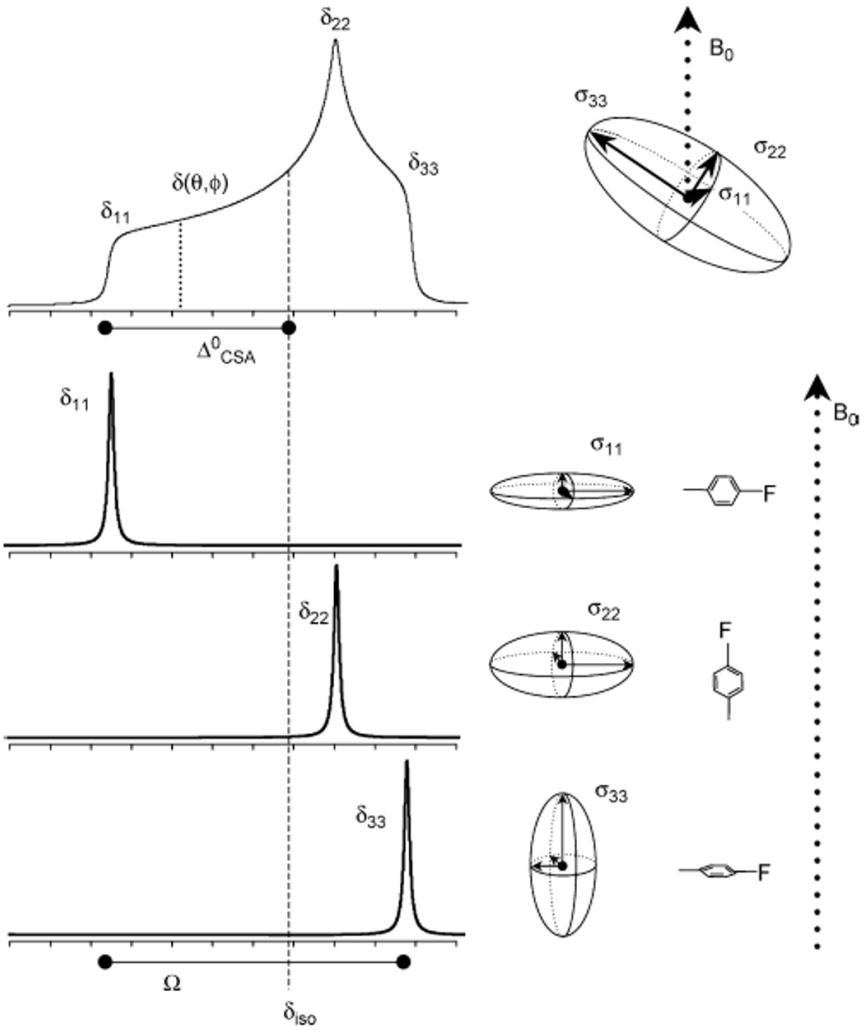

Figure 1.12: One molecule can contribute to multiple signals in NMR spectra by being recorded at multiple orientations. These orientations contribute to a signal distribution made up of each orientational element. Figure from [31].

chemical shifts due to the specific orientations of the nuclei in the studied sample (see figure 1.12). Mathematically, the different orientations are described by tensors, whose elements in the principle axis frame (PAF) are σ_{11}, σ_{22}, and σ_{33}.

1.8 Deuterium NMR

Deuterium NMR gets more complex due to its characteristic spin of 1. Quadrupolar nuclides are defined as having a spin (I) greater than ½ and are affected by their electric quadrupolar moment. This quadrupolar moment (eQ) describes the effective shape of the ellipsoid of nuclear charge distribution [32]. Its interaction with the nuclear spin along the C-D

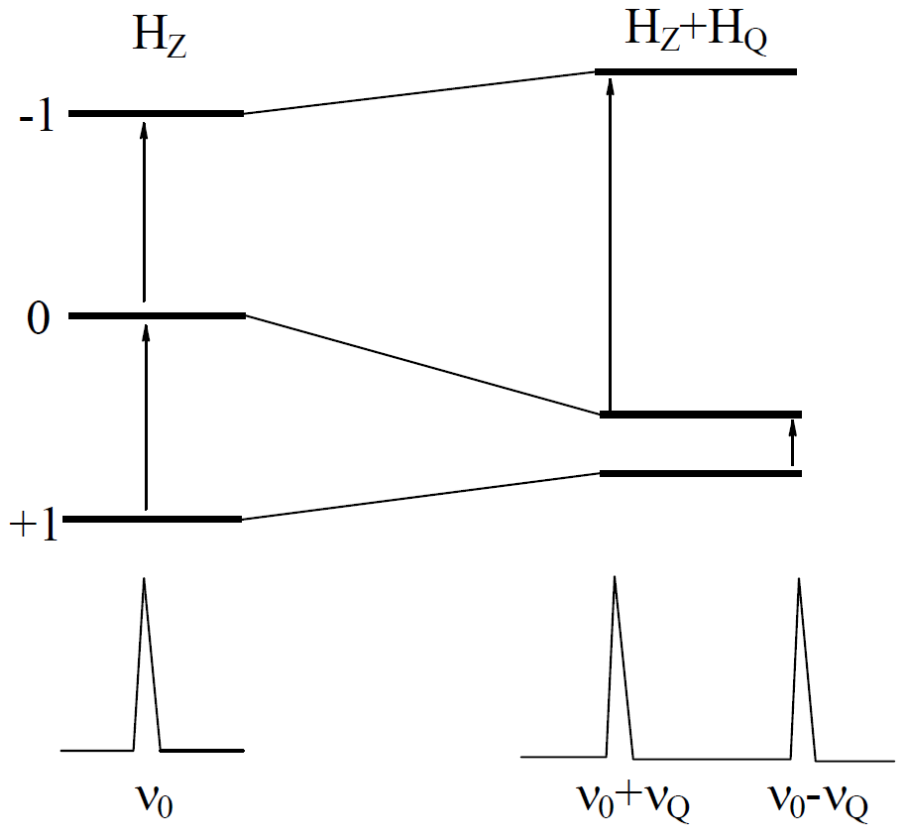

Figure 1.13: The energy state transitions of deuterium are shown. A simple interpretation of energy states is on the left (it only has a factor of the splitting energy state Zeeman effect, H_Z), and the added effects of the quadrupole moment's interaction (H_Q) is displayed on the right. Figure from [33].

bond associated with eQ in the case of deuterium (spin 1) shifts each of the three energy states it can occupy (+1, 0, -1) by an amount described by,

$$E_m = (\frac{e^2qQ}{4I(2I-1)})[3m^2 - I(I+1)][\frac{1}{2}(3cos^2\theta - 1) + \frac{1}{2}\nu sin^2\theta cos2\phi] \tag{1.5}$$

where q is the field gradient and v is the asymmery parameter. The allowed transitions +1 $\longleftrightarrow$ 0 and 0 $\longleftrightarrow$ -1 are affected and look like figure 1.13, consisting of a doublet separated by quadrupole splitting Δv_Q,

$$\Delta v_Q = \frac{3}{4}\frac{e^2qQ}{h}[3cos^2\theta - 1 - \nu sin^2\theta cos2\Phi] \tag{1.6}$$

The electric quadrupole moment effectively causes multiple signals on the NMR spectrum of spin 1 deuterium [33, 34, 35].

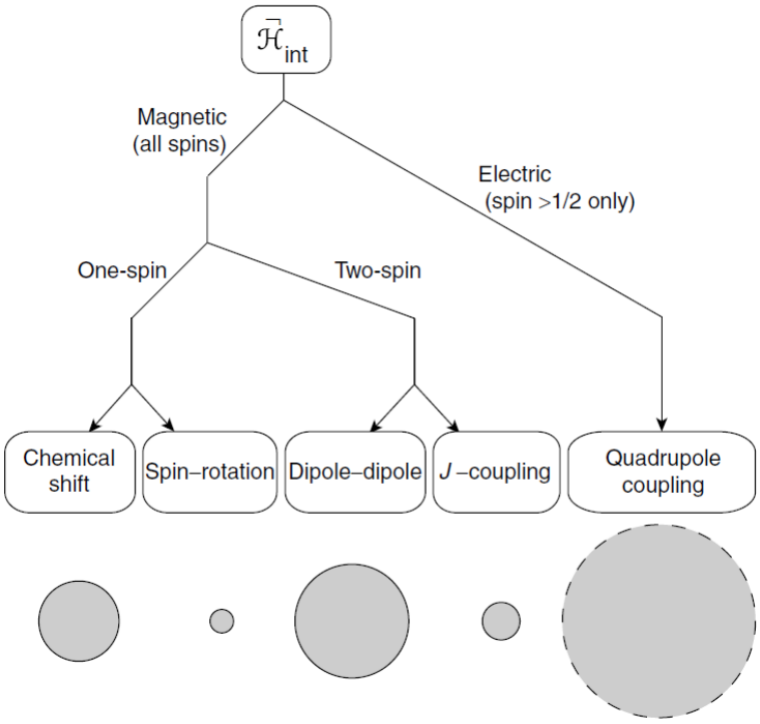

Figure 1.14: The Hamiltonian for Internal Spin Interactions. Quadrupole coupling interactions dominate the contribution [36].

1.9 Features of Deuterium NMR

Deuterium NMR is especially useful due to the measurement of quadrupole coupling interactions. As briefly stated earlier, deuterium (particles with spin $> 1/2$) has a quadrupole moment which interacts with the electric field gradient (EFG, which describes the local electronic environment). The interaction between the quadrupole moment and the EFG contribute the NMR interaction component of quadrupole coupling, as can be seen in figure 1.14. This interaction is the most important in deuterium NMR, and is highly sensitive to the symmetry and time scale of molecular motion. For instance, refer back to the orientational dependence of equations 1.5 and 1.6. The emitted energy is described by the orientation of the C-D bonds to the axis of rotation (see figure 1.15).

The other energy components of the NMR spectra are described in greater detail for ^{1}H NMR, but shall be briefly described. The chemical shift is the resonant frequency of a nucleus relative to a standard in a magnetic field. Spin rotation describes the local magnetic field

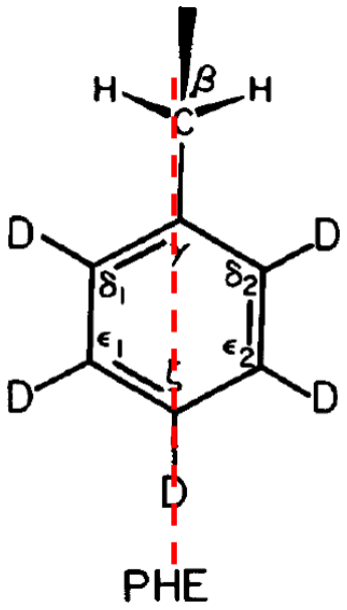

Figure 1.15: A deuterium labeled Phenylalanine residue, with an example rotation about the axis [35].

generated by the circular motion of electrons in a rapid rotating molecule [37]. Dipole-dipole interactions describe the interactions directly between magnetic dipoles through space. J-Coupling describes indirect magnetic interactions of nuclear spins with each other, through the involvement of electrons (e.g. through bonds). Quadrupole coupling has the highest relative magnitude of these interactions. In addition, on Phenylalanine the deuterium signal is four times as strong since the four C-D bond orientations are symmetrical respective to the axis of rotation (all four contribute to the same signal). However, dipole-dipole coupling still has a relatively strong magnitude which can perturb the spectra. Accordingly, magic angle spinning can be used to average out the dipole-dipole interactions to zero.

1.10 Magic Angle Spinning (MAS)

Spinning the sample at an angle where $cos^2\theta_m = 1/3$ eliminates any interaction that depends on the second Legendre polynomial (like dipole-dipole interactions). θ_m is about 54.74° with respect to the static external magnetic field B_0 (see figure 1.16). Spinning the sample at θ_m results in a splitting of the static line shape into side-bands equal to the spinning frequency

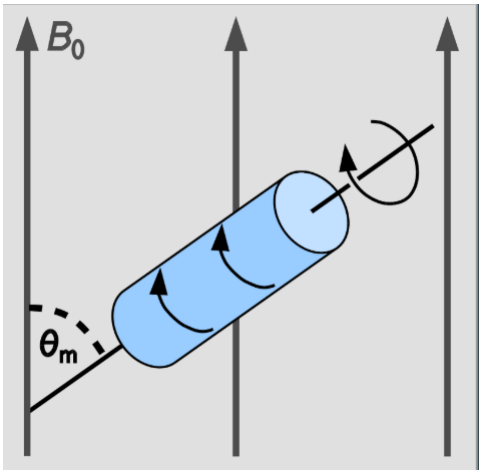

Figure 1.16: Image of the magic angle θ_m [38].

(see figure 1.17 for reference).

1.11 Structural Analysis of P1

The computer program Xplor-NIH is a software package for NMR biomolecular structure determination [39]. Using this program, Dr. Alex Greenwood, NMR specialist at William & Mary, performed analysis of p1 bound to Ni^{2+} (see figure 1.18) to resolve a clear image of its structure and orientation relative to the lipid bilayer. The peptide is analyzed in coordination with Ni^{2+} and not Cu^{2+} due to copper's paramagnetic perturbation of NMR signal.

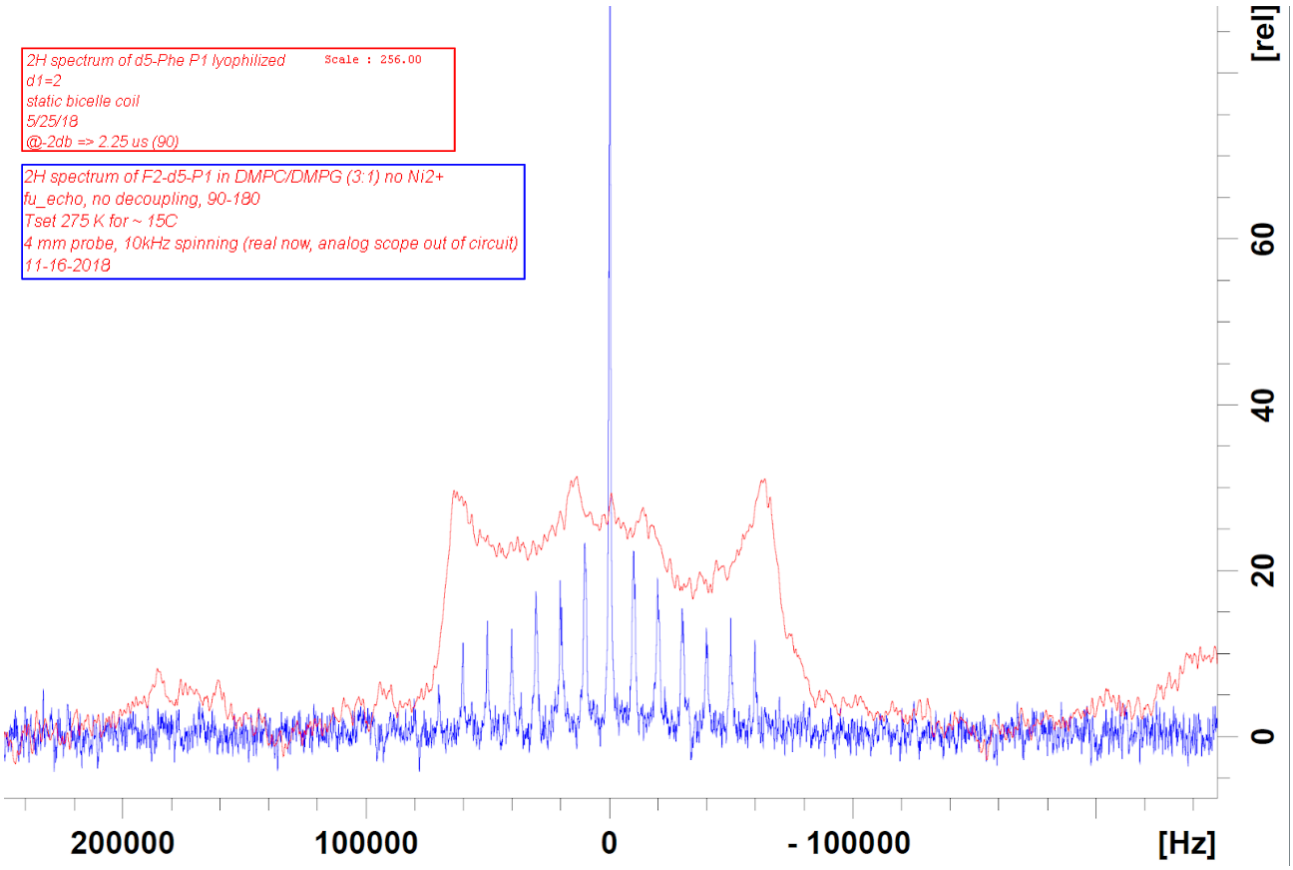

Figure 1.17: ^{2}H NMR data of F2-d5-p1. In red is the static spectra of lyophilized F2-d5-p1 powder. In blue is MAS spectra of F2-d5-p1 non-metallated and bound to 3:1 DMPC/DMPG. The two spectra are not static and MAS data of the same sample, but simply serve to represent the splitting of a static line shape into side bands during a MAS experiment [40].

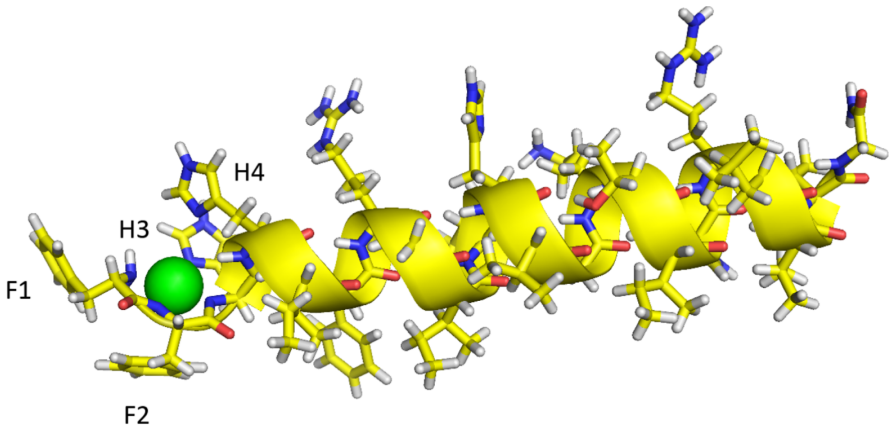

Figure 1.18: The structure determined above for p1 was acquired by Dr. Alex Greenwood through input of NMR data constraints (data acquired through the Cotten lab) alongside simulation of annealing and molecular dynamics with the program Xplor. The structure highlights the ATCUN motif previously described. The black bar at the bottom represents the orientation of the lipid bilayer. Figures courtesy of Dr. Greenwood.

Chapter 2

Experimental Approach

2.1 Peptide Synthesis & Purification

Crude ^{2}H labeled peptides were acquired from the University of Texas Southwestern Medical Center. The peptides were purified by high-performance liquid chromatography (HPLC) with a 0.1% trifluoroacetic acid (TFA) and 15% acetonitrile nanopure water solution through a Waters C-18 column. The samples were ran through the column in quantities of $\approx$ 5mL with a concentration of 2-3mg/mL. The samples were then rotovapped to evaporate solvents used in HPLC. Subsequently, the aqueous samples were frozen with liquid nitrogen and lyophilized into powders. The next step in the process was removal of TFA from the purified peptides (TFA was used in HPLC but rotovaporization is not able to remove it). Adding HCl allowed chloride ions to remove TFA that was ionically bound to the positive charges along the peptide. The samples were then lyophilized again. In order to remove excess chloride ions, the samples were brought to physiological pH to remove the positive charge from the peptide, then run through steps of dialysis to remove excess chloride ions no longer bound. Post-dialysis, the peptides (if desiring a metallated sample) were metallated by adding 0.1M $NiCl_2$ solution to the peptide at a 1:1 ratio of peptide:Ni. The lipids were then prepared by mixing DMPC:DMPG lipids at a 3:1 ratio in water, incubating them at 40°with the peptide. In the case of unoriented sample NMR that was used for F2(d5)-p1 and F1(d5)-p1, after incubation of the lipid films, they are

pipetted out and immediately centrifuged still within the pipette tip and lyophilized. After complete dehydration, the samples are packed into an NMR rotor and re-hydrated with 45% D2O depleted water.

2.2 Data

Samples of F2-d5-p1 were prepared metallated and non-metallated. Samples of non-metallated F1-d5-p1 were also purified as a control to further analyze dynamics. Experimental ssNMR data was collected and fit by NMR research specialist Dr. Alex Greenwood with the aid of Bruker's program TopSpin 4.0.5. To begin, sample preparation hydrated the peptides in the presence of lipid bilayers with D2O depleted water, to reduce the natural presence of deuterium in the sample from that of normal hydration. The deuterium from the D2O in the water affects the center band at 0Hz in the NMR spectra. Unfortunately, this means that any analysis of the spectra around 0Hz is not significant. Figure 2.1 displays the ^{2}H spectrum of non-metallated F2-d5-P1 in 3:1 DMPC/DMPG. Clear signal and resolution is achieved. We can see a clear gap between the noise band and the side-bands generated from the deuterium labeled Phenylalanine side chain. The signal seems to be symmetric as we should expect from a symmetrical axis of rotation and the magic angle spinning side bands are spaced 10kHz apart (equal to the spinning frequency). We most likely expect, due to the symmetry of the side bands, that the farthest right hand peak was lost in the noise. Moving forward, figure 2.1 shows the ^{2}H spectrum of metallated F2-d5-P1, also in 3:1 DMPC/DMPG. The magnitude is about 4x smaller on a scale relative to the spectrum displayed in figure 2.1. In this, experimental run it is harder to distinguish between the outer side bands and the noise of the experiment. Overlap figure 22, the metallated and the non-metallated experimental runs: the outer edges of the side bands appear to collapse into noise at around the same $\approx$ 60kHz.

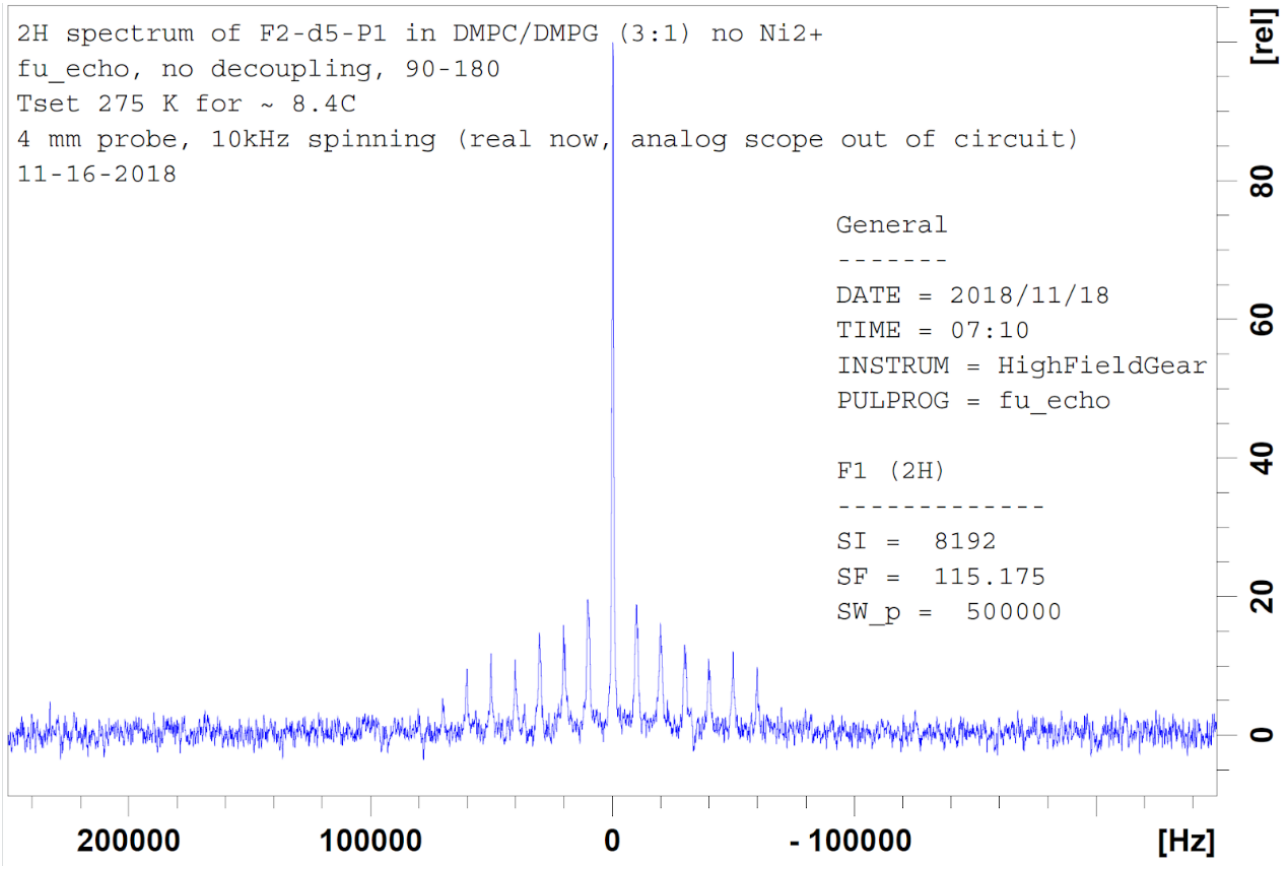

Figure 2.1: ^{2}H spectrum of non-metallated F2-d5-P1 in 3:1 DMPC/DMPG. Acquisition time 0.0081920 seconds, Number of scans 512000 [40].

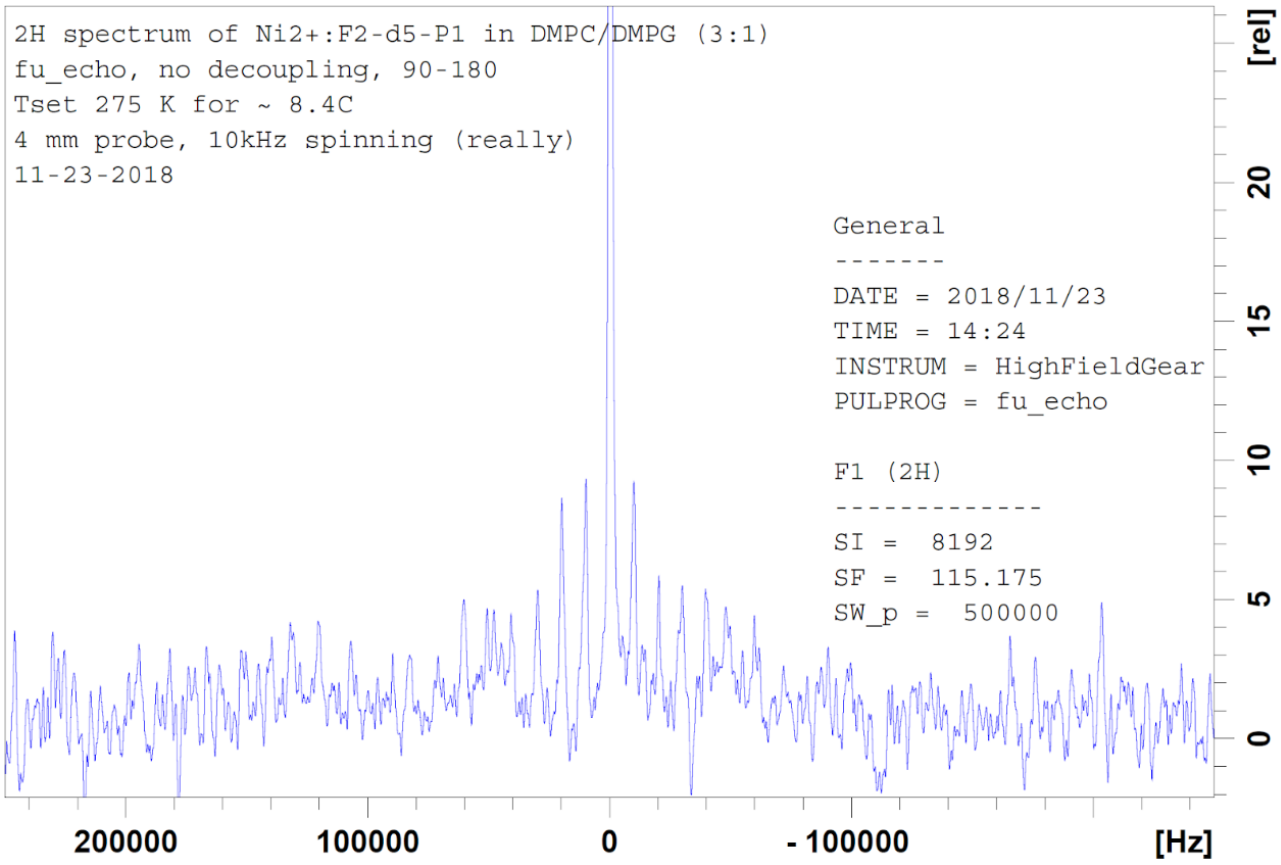

Figure 2.2: ^{2}H spectrum of metallated F2-d5-P1 in 3:1 DMPC/DMPG. Acquisition time 0.0081920 seconds, Number of scans 1024000 [40].

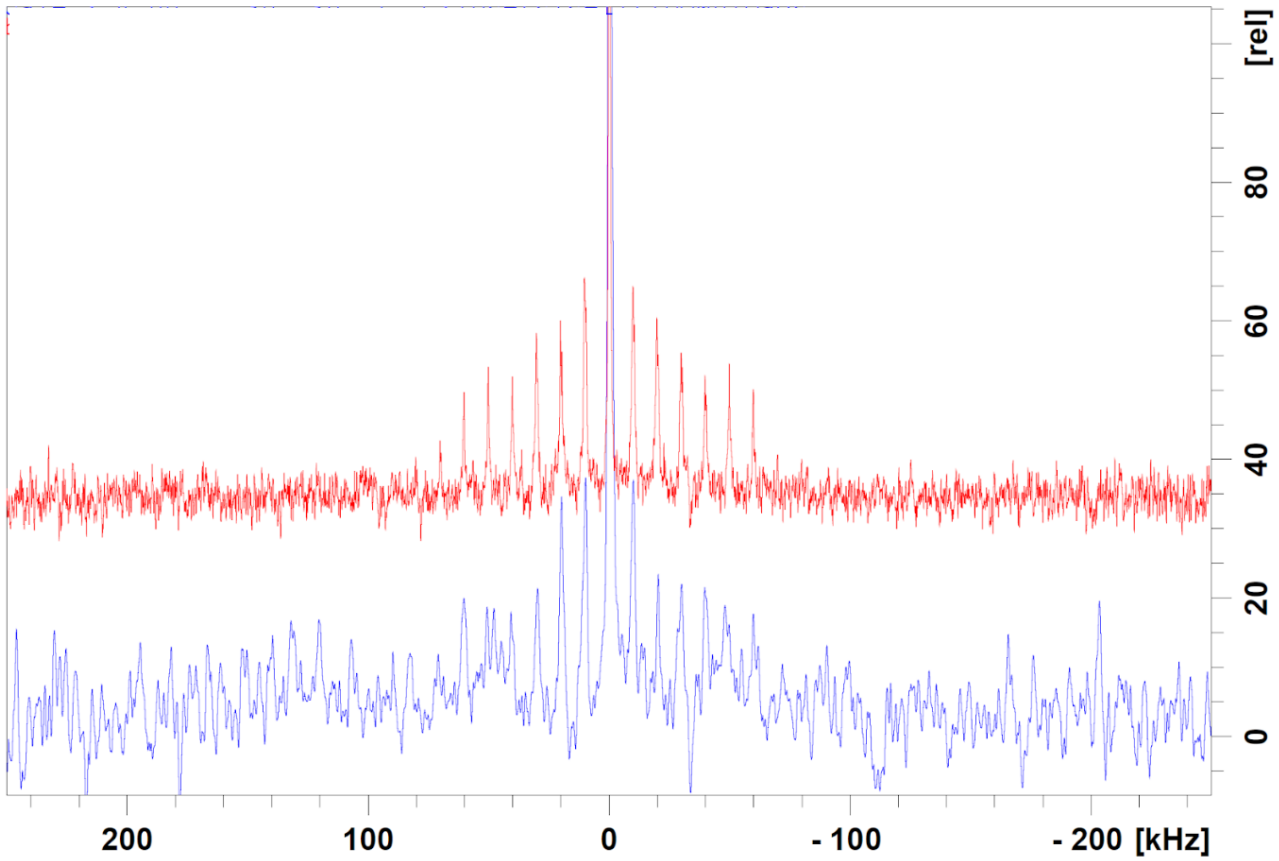

Figure 2.3: Overlapped ^{2}H spectra of figures 2.1 and 2.2 displaying (red) non-metallated F2-d5-P1 and (blue with a Scale 4.0) for metallated F2-d5-P1. Both samples comprised of peptide and lipids 3:1 DMPC/DMPG [40].

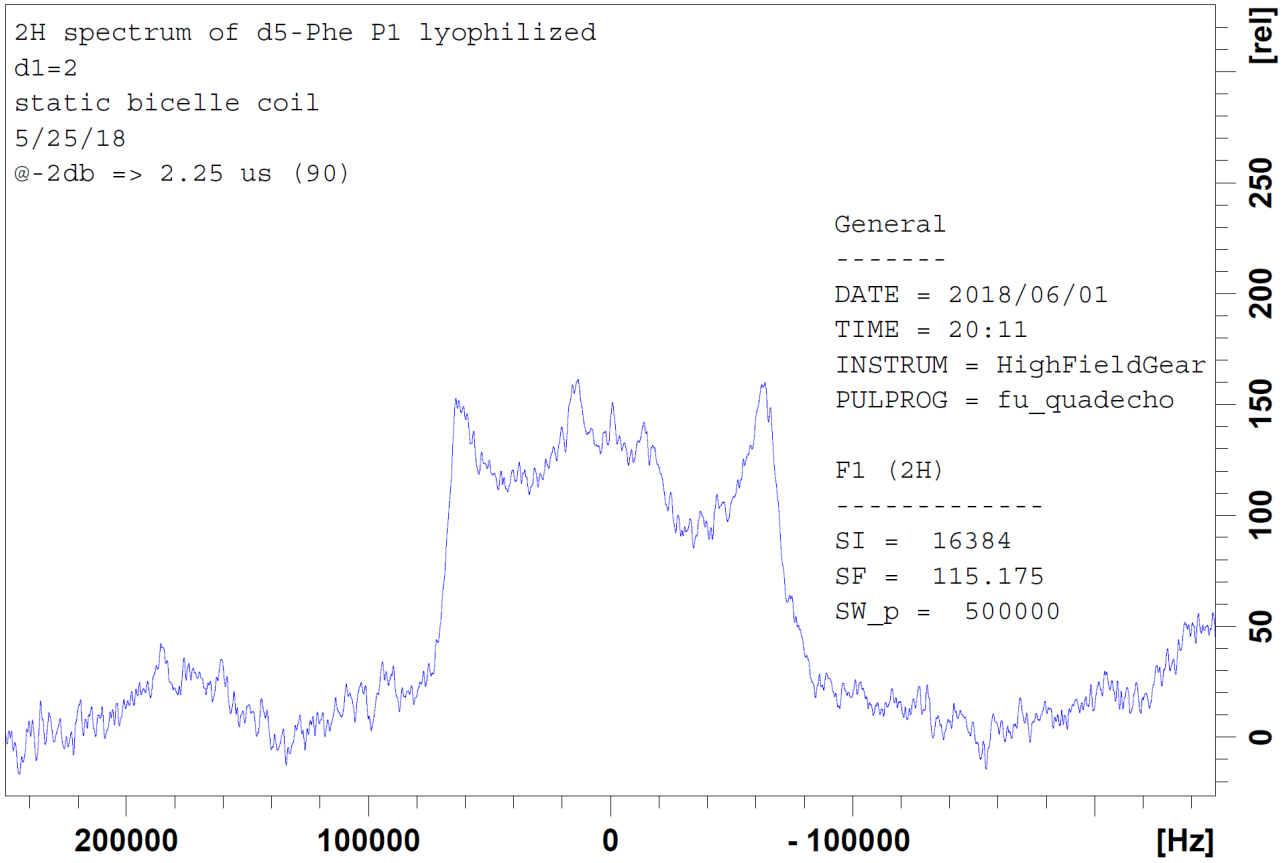

Figure 2.4: ^{2}H spectrum of lyophilized F2-d5-P1 without the presence of a lipid bilayer [43].

2.3 ^{2}H NMR Data Analysis

The computer program EXPRESS (EXchange Program for RElaxing Spin Systems) simulates the effects of Markovian jump dynamics for a wide variety of solid state nuclear magnetic resonance experiments [41]. EXPRESS thus offers a tool of computational analysis for ^{2}H data. As an example of the parameters that a program such as EXPRESS uses to simulate NMR, I refer to data analysis of Phenylalanine side chains in the mineral-recognition domain of the biomineralization protein Statherin [42]. Deuterium labeled F7 and F14 were analyzed using ^{2}H MAS NMR to investigate dynamics of the surface-adsorbed fragment of the Statherin protein. The labeling and experimental parameters utilize nomenclature referenced in figure 2.5. The study compared experimental NMR data with NMR simulations (figure 2.6) generated with the parameters seen in figure 2.7. To well explain the utility of these simulations, I start by defining the parameters at hand. The QCC (kHz) represents the Quadrupole Coupling Constant, which is defined as $\frac{e^2qQ}{\hbar}$ and seen in the equations 1.5 and

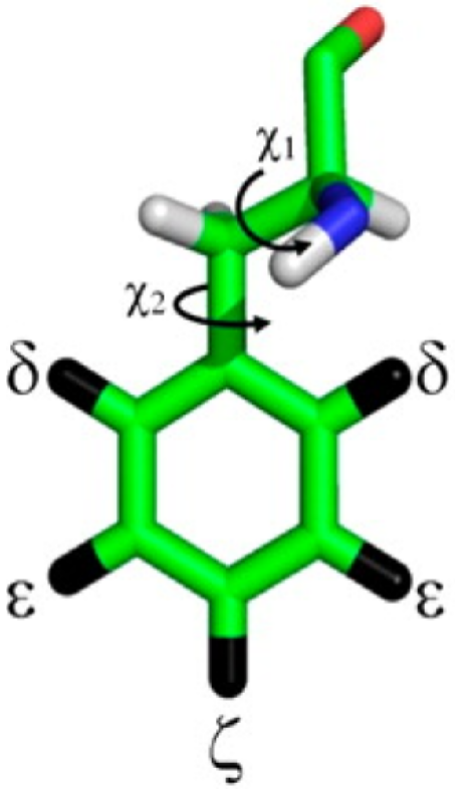

Figure 2.5: Phenylalanine model meant to represent the rotational parameters χ_1 and χ_2 used in molecular dynamics simulations for F7 and F14 [42].

1.6. The asymmetry parameter (ν) defines the asymmetry of the principle axis tensors. Axial symmetry would have $\nu = 0$ whereas other sources define $\nu = \frac{\sigma_{22}-\sigma_{11}}{\sigma_{33}-\sigma_{iso}}$. The rotamer exchange rate constant describes the rate at which potential rotamers (conformers distinct from one another by rotation of χ_1 and χ_2) of the phenylalanine residue shift. The ring flipping rate constant describes the rate at which the Phenylalanine ring flips about the axis of rotation about χ_2. Adjustment of these parameters can yield information about the phenylalanine residue population percentage of a particular orientation. There are competing theories as to which parameterization technique yields the most accurate results. For instance, whether it is better to tune the population values while keeping constant the rotamer exchange rate or to do the opposite by tuning the rotamer exchange rate and keeping constant the population values. The end goal is to achieve a simulated NMR spectrum which best matches the experimental NMR spectrum. Consequently, the fixed parameters of the best fit inform on the dynamics. In our case, the parameters determined for the non-metallated sample can be compared to those of the metallated sample, or to other residues (e.g. a nearby F1 which can also be deuterium

labeled).

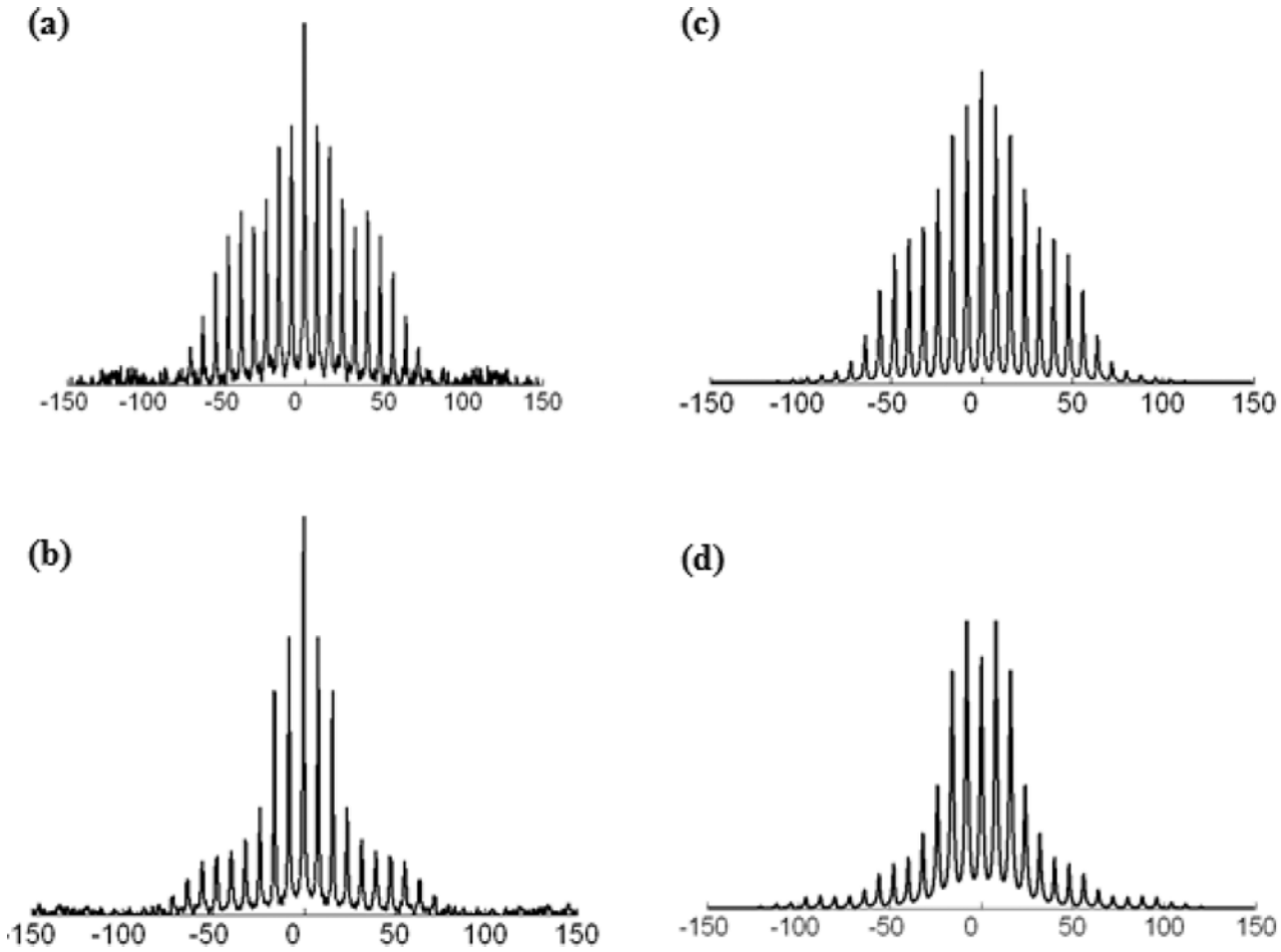

Figure 2.6: NMR spectrum from the study of Statherin. ^{2}H MAS spectra both experimental and simulated of bound F7 and F14. (A) Experimental F7; (B) Experimental F14; (C) Simulated F7; (D) Simulated F14 [42].

2.4 Results

Preliminary results of simulations matching experimental lyophilized F2-d5-p1 powder spectra can be seen in figure 2.8. The EXPRESS program parameters agreed with the experimental data with the following constraints: Fast phenyl π-flips ($k \leq 10^9 s^{-1}$) in *trans* conformation, Slow phenyl π-flips ($k \geq 10^3 s^{-1}$) in *gauche* conformation , Slow ($k \leq 10^4 s^{-1}$) g^+-t-g^- jumps, Unequal populations: g^+-t-g^- $\approx$ 1:0.3:1. [43].

parameters for HAP-bound phenylalanines	F7 ζ deuteron	F7 δ/ε deuterons	F14 ζ deuteron	F14 δ/ε deuterons
QCC (kHz)	183.0	183.0	182.3	182.3
asymmetry parameter	0.06	0.06	0.06	0.06
rotamer exchange rate constant (s^{-1})	5×10^6	5×10^6	6×10^6	6×10^6
ring flipping rate constant (s^{-1})	none	5.6×10^9	none	2.6×10^9
F7 conformers	χ_1 (deg)	χ_2 (deg)	population (%)	
conformer1	186.2	88.6	76.1	
conformer2	274.7	54.8	23.9	
F14 conformers	χ_1 (deg)	χ_2 (deg)	population (%)	
conformer1	93.1	208.8	40.9	
conformer2	273.6	56.8	59.1	

Figure 2.7: Parameters used to simulate ^{2}H MAS NMR line shapes in figure 2.6 [42].

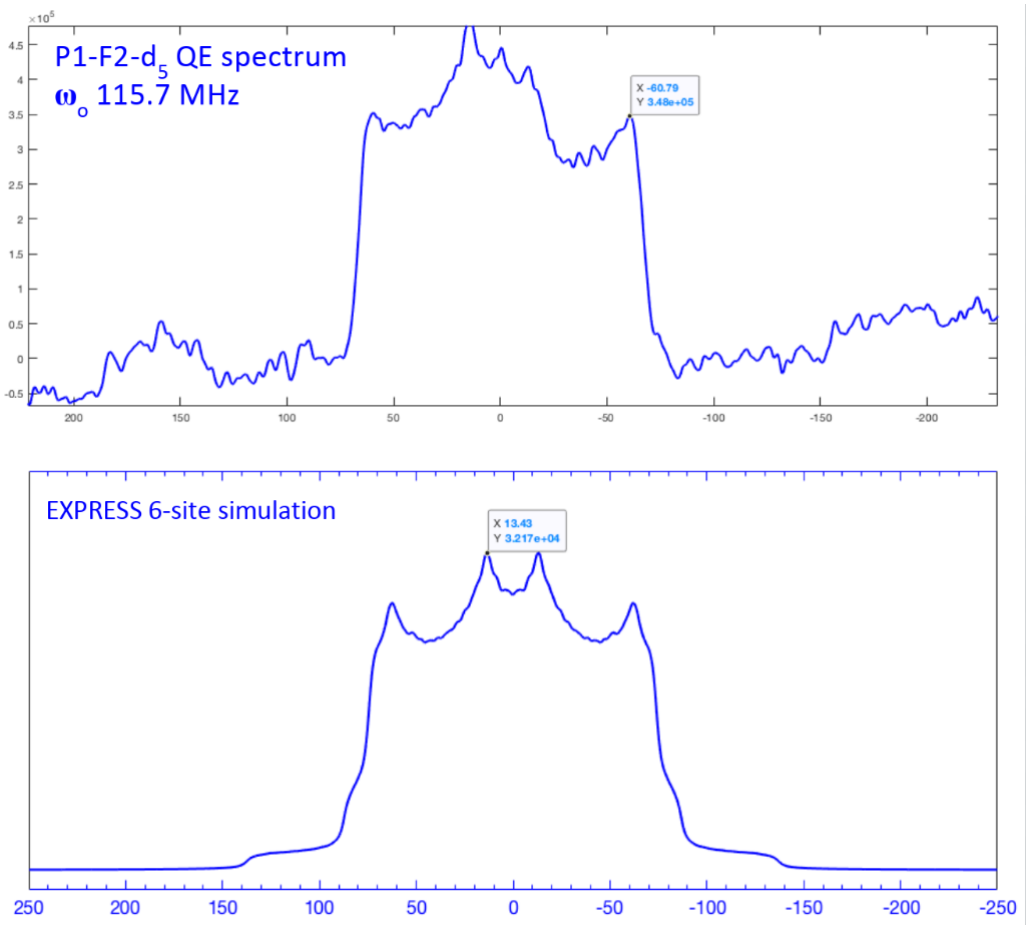

Figure 2.8: Experimental lyophilized F2-d5-p1 powder spectrum above an EXPRESS-simulated NMR spectrum of F2-d5-p1 [43].

Chapter 3

Conclusion

3.1 Summary

Preliminary investigation into the rotational dynamics of F2 in Piscidin 1 indicates that the host defense peptide is predisposed to membrane binding such that no conformational changes are outright evident from the ^{2}H MAS ssNMR data of non-metallated peptide with a F2 deuterium labeled side chain compared to that of the metallated peptide.

3.2 Applications

A higher understanding of the dynamics of the host defense peptide Piscidin 1 will help in the development of synthetic HDPs, in recognizing mechanistic interactions of all HDPs which localize to bacterial membranes, and in contextualizing known models of peptide or protein active sites.

3.3 Future Work

The dynamics involved in the active site of Piscidin 1, and Piscidin 3, can be explored more thoroughly with analysis of F1-d5-P1, the Histidine at position 4, and comparison of dynamics with P3 or mutated forms of P1. The power of the EXPRESS program, or other molecular dynamics programs, to parameterize molecular dynamics simulations gives future deuterium NMR dynamics simulations a strong foundation to investigate rotational dynamics.

Bibliography

[1] Perrin; et. al; High-Resolution Structures and Orientations of Antimicrobial Peptides Piscidin 1 and Piscidin 3 in Fluid Bilayers Reveal Tilting, Kinking, and Bilayer Immersion. *J. Am. Chem. Soc.* **2014**, *136*, 3491-3504.

[2] Fjell, C; Hiss, J; Hancock, R; Schneider, G; Designing Anti-Microbial Peptides: Form Follows Function. *Nature Reviews, Drug Discovery.* **2012**, *11*, 37-51.

[3] Hayden, Robert M.; et. al; "Complementary Effects of Host Defense Peptides Piscidin 1 and Piscidin 3 on DNA and Lipid Membranes: Biophysical Insights into Contrasting Biological Activities". *The Journal of Physical Chemistry B*, **2015**, *119*, 15235-15246.

[4] Lauth, X.; et al.; Discovery and Characterization of Two Isoforms of Moronecidin, a Novel Antimicrobial Peptide from Hybrid Striped Bass. *J. Biol. Chem.* **2002**, *277*, 5030-5039.

[5] Review on Antimicrobial Resistance. Tackling Drug-Resistant Infections Globally: Final Report and Recommendations. May 2016.

[6] Chinchar, V.G.; et. al; "Inactivation of viruses infecting ectothermic animals by amphibian and piscine antimicrobial peptides" *Virology.* **2004**, *323*, 268-275.

[7] Wang, Guangshun; *Pharmaceuticals.* **2013**, *6*, 728-758.

[8] Silphaduang, U.; Noga, E.; Peptide Antibiotics in Mast Cells of Fish. *Nature.* **2001**, *414*, 268-269.

[9] Andrews, J.M.; *J Antimicrob Chemother.*. **2001**, *48*, Suppl 1:5-16.

[10] Wang, Guangshun; Li, Xia; Wang, Zhe; "APD2: the updated antimicrobial peptide database and its application in peptide design". *Nucleis Acids Research*, **2008**, *37*, D933-D937.

[11] Vogt, T. C. B.; Bechinger, B.; "The Interactions of Histidine-containing Amphipathic Helical Peptide Antibiotics with Lipid Bilayers". *The Journal of Biological Chemistry.* **1999**, *274 (41)*, 29115-29121.

[12] Mulero, I.; et. al; "The antimicrobial peptides piscidins are stored in the granules of professional phagocytic granulocytes of fish and are delivered to the bacteria-containing phagosome upon phagocytosis". *Developmental and Comparative Immunology.* **2008**, *32*, 1531-1538.

[13] Chekmenev; et. al; Investigating Molecular Recognition and Biological Function at Interfaces Using Piscidins, Antimicrobial Peptides from Fish. *Biochim. Biophys. Acta.* **2006**, *1758*, 1359-1372.

[14] Seelig, J.; Thermodynamics of Lipid-Peptide Interactions. *Biochim. Biophys Acta.* **2004**, *1666*, 40-50.

[15] Oren, Ziv; Shai, Yechiel; Cyclization of a Cytolytic Amphipathic R-Helical Peptide and Its Diastereomer: Effect on Structure, Interaction with Model Membranes, and Biological Function". *Biochemistry.* **2000**, *39*, 6103-6114.

[16] Cheng, J.T.J.; et. al; "The importance of bacterial membrane composition in the structure and function of aurein 2.2 and selected variants". *Biochimica et Biophysica Acta*, **2011**, *1808*, 622-633.

[17] Murzyn, Kryzsztof; Róg, Tomasz; Pasenkiewicz-Gierula, Marta; "Phosphatidylethanolamine-Phosphatidylglycerol Bilayer as a Model of the Inner Bacterial Membrane". *Biophysical Journal*, **2005**, *88*, 1091-1103.

[18] National Center for Biotechnology Information. PubChem Compound Database; CID=5497103, https://pubchem.ncbi.nlm.nih.gov/compound/5497103 (accessed Dec 2, 2018).

[19] National Center for Biotechnology Information. PubChem Compound Database; CID=5283509, https://pubchem.ncbi.nlm.nih.gov/compound/5283509 (accessed Dec 2, 2018).

[20] National Center for Biotechnology Information. PubChem Compound Database; CID=131562, https://pubchem.ncbi.nlm.nih.gov/compound/131562 (accessed Dec 2, 2018).

[21] National Center for Biotechnology Information. PubChem Compound Database; CID=46891824, https://pubchem.ncbi.nlm.nih.gov/compound/46891824 (accessed Dec 2, 2018).

[22] Libardo; et. al; Nuclease Activity Gives an Edge to Host-Defense Peptide Piscidin 3 Over Piscidin 1, Rendering It More Effective Against Persisters and Biofilms. *The FEBS Journal.* **2017**, *284*, 3662-3683.

[23] Harford, C; Sarkar, B; Amino Terminal Cu(II)- and Ni(II)-Binding (ATCUN) Motif of Proteins and Peptides: Metal Binding, DNA Cleavage, and Other Properties. *Acc Chem Res.* **1997**, *30*, 123-130.

[24] Fang, Y.; et. al; "Diastereoselective DNA Cleavage Recognition by Ni(II)*Gly-Gly-His-Derived Metallopeptides". *J. Am. Chem. Soc.*, **2006**, *128*, 3198-3207.

[25] Jin, Yan; Cowan, J.A.; "DNA Cleavage by Copper-ATCUN Complexes. Factors Influencing Cleavage Mechanism and Linearization of dsDNA". *J. Am. Chem. Soc.*, **2005**, 8408-8415.

[26] Wang, Ting-Yi; et. al.; "Membrane oxidation in cell delivery and cell killing applications". *ACS Chem Biol.*, **2017**, *12(5)*, 1170-1182.

[27] Libardo, M. Daben J.; et. al; "How does membrane oxidation affect cell delivery and cell killing?" *Trends Biotechnol.*, **2017**, *35(8)*, 686-690.

[28] Young, I. S.; McEneny, J.; "Lipoprotein oxidation and atherosclerosis". *Biochemical Society Transactions*, **2001**, 358-362.

[29] Claridge, T.D.W.; *High-Resolution NMR Techniques in Organic Chemistry: Second Edition*. **2009**.

[30] Mujeeb, Khan; Structural transformations related to organic solid-state reactions: correlation studies of NMR and X-ray analysis. **2008**, Figure 3.3.

[31] *Progress in Nuclear Magnetic Resonance Spectroscopy*, **2005**, *6 (46)*, 1-21.

[32] Apperley, David C.; Hodgkinson, Paul; Harris, Robin K.; "Solid-State NMR : Basic Principles and Practice". **2012**, 140-141.

[33] University College London. NMR Lecture Notes: 10. Solid State NMR. **21 May 2014**, accessed 9 October 2018. *https* : *//www.ucl.ac.uk/nmr/NMR_lecture_notes*.

[34] Asakura, Tetsuo; Ando, Isao; "Studies in Physical and Theoretical Chemistry: Solid State NMR of Polymers". **1998**, 192-194.

[35] Kinsey, R; Kintanar, A; Oldfield, E; Dynamics of Amino Acid Side Chains in Membrane Proteins by High Field Solid State Deuterium Nuclear Magnetic Resonance Spectroscopy. *The Journal of Biological Chemistry*. **1981**, *256(17)*, 9028-9036.

[36] Levitt, Malcolm H.; "Spin Dynamics". **2001**.

[37] https://www.chem.wisc.edu/areas/reich/nmr/08-tech-01-relax.htm

[38] *https://en.wikipedia.org/wiki/Magic$_a$ngle$_s$pinning*

[39] Schwieters, Charles D.; et. al; "The Xplor-NIH NMR molecular structure determination package". *Journal of Magnetic Resonance*, **2003**, *160*, 65-73.

[40] Greenwood, Alex; Cotten, M.; Retrieved from author. TopSpin NMR files.

[41] Vold, Robert L.; Hoatson, Gina L.; "Effects of jump dynamics on solid state nuclear magnetic resonance line shapes and spin relaxation times". *Journal of Magnetic Resonance*, **2009**, *198*, 57-72.

[42] Li, K.; Emani, P. S.; Ash, J; Groves, M.; Drobny, G.P.; "A Study of Phenylalanine Side-Chain Dynamics in Surface-Adsorbed Peptides Using Solid-State Deuterium NMR and Rotamer Library Statistics". *J. Am. Chem. Soc.*, **2014**, *136*, 11402-11411.

[43] Dr. Robert L. Vold, retrieved from author.